

Analytically Tractable Hidden-States Inference in Bayesian Neural Networks

LUONG HA NGUYEN^{*,†} and JAMES-A. GOULET^{*,†}

Department of Civil, Geologic and Mining Engineering
POLYTECHNIQUE MONTRÉAL, CANADA

Abstract

With few exceptions, neural networks have been relying on back-propagation and gradient descent as the inference engine in order to learn the model parameters, because the closed-form Bayesian inference for neural networks has been considered to be intractable. In this paper, we show how we can leverage the *tractable approximate Gaussian inference*'s (TAGI) capabilities to infer hidden states, rather than only using it for inferring the network's parameters. One novel aspect it allows is to infer hidden states through the imposition of constraints designed to achieve specific objectives, as illustrated through three examples: (1) the generation of adversarial-attack examples, (2) the usage of a neural network as a black-box optimization method, and (3) the application of inference on continuous-action reinforcement learning. These applications showcase how tasks that were previously reserved to gradient-based optimization approaches can now be approached with analytically tractable inference.

1 Introduction

With few exceptions, neural networks have been relying on backpropagation [16] and gradient descent as the inference engine in order to learn the model parameters. In such a case, the inference can be seen as approximating the posterior by a point solution minimizing a loss function. In addition to learning the model parameters, one may be interested in inferring the values of hidden states in a neural network. Note that we are not interested here in cases such as variational auto-encoder [11], or in generative adversarial networks

^{*}Equal contribution

[†]Correspondence: luongha.nguyen@gmail.com, james.goulet@polymtl.ca

[7, 4] where dedicated latent variables are added; we are rather interested in inferring the value of hidden states from single observation instances. A first example is the case of adversarial attacks (AA), where images can be tailored in order to fool a neural network into performing incorrect classifications with high certainty [8]. In the context of white-box AA, images that seem realistic for a human observer, are generated by inferring perturbations that can be added to the input layer of a neural network in order to fool it. A second example of hidden state inference involves the definition of policy networks in reinforcement learning (RL) with methods such as advantage actor critic (A2C) [13] and proximal policy optimization (PPO) [17]. For such cases, current methods relying on backpropagation use gradient ascent in order to infer the optimal actions that are maximizing an action-value function [18].

The closed-form Bayesian inference for neural networks has long been considered to be intractable, both in terms of its parameters [6] or hidden states [2, 12]. Recently, the *tractable approximate Gaussian inference* (TAGI) [10] method was shown to either match or exceed the performance of neural networks trained with backpropagation in fully connected architectures [10], for convolutional (CNN) and generative ones [15], as well as for deep reinforcement learning with categorical actions [14]. This paper shows how we can leverage TAGI’s probabilistic inference capabilities to infer hidden states, rather than only using it for inferring the network’s parameters. One novel aspect introduced is the capacity to infer hidden states through the imposition of constraints designed to attain specific objectives, as illustrated in this paper through three examples: (1) the generation of adversarial-attack examples, (2) the usage of a neural network as a black-box optimization method, and (3) the application of inference on continuous-action reinforcement learning. The paper is organized such that before diving in the theory and examples for these applications in Sections 3-5, Section 2 reviews the theory behind TAGI.

2 Tractable Approximate Gaussian Inference

The tractable approximate Gaussian inference method relies on a two step *forward-backward* process. In the *forward* process, the uncertainty from the input layer is propagated through the hidden layers along with the uncertainty associated with model parameters, i.e., the weights and biases. The forward propagation of uncertainty allows forming the joint prior knowledge between successive pairs of hidden layers as well as between hidden layers and the parameters directly connecting into it. This process involves two approxi-

mations: first, that the product of a Gaussian hidden unit and a Gaussian weight parameter is also Gaussian, and second that non-linear activation functions can be locally linearized at the expected value of the hidden unit. Previous applications on validation benchmarks have confirmed that these approximations still allow matching or exceeding state-of-the-art performance on a same architecture trained with gradient descent and backpropagation [10, 15, 14].

The *backward* process corresponds to the inference step that is based on the Gaussian conditional equations. In order to maintain a linear computational complexity during inference, we take advantage of the inherent conditional independence between the hidden layers of a neural network. This enables performing the layer-wise inference from successive pairs of hidden layers and from hidden layers to the parameters that connect into it.

In the experimental setups explored so far, the inference capacity of TAGI was employed to learn the neural network parameters whereas the updated knowledge regarding the hidden units is discarded each time new training observations become available. In the current setup, we are not only interested in using TAGI to infer the network’s parameters, but also the hidden units at specific location within the network. The appeal of TAGI is that it can inherently do so, without requiring any modifications to its formulation. In the following subsections, we will present how the novel inference capacity from the TAGI method can be leveraged in order to provide new solutions to existing challenges such as adversarial-attack generation, black-box optimization, and continuous-action reinforcement learning.

3 Adversarial Attack through Inference

In the first example, we are interested in white-box adversarial attacks [1] where we have access to the network and its parameters. Current white-box attacks are typically formulated as an optimization problem where one uses gradient descent and backpropagation in order to find optimal perturbations to be applied on the input layer in order to fool the network into making wrongful classifications.

With TAGI, the generation of adversarial-attack images can be done analytically, without relying on an optimization process. We start with the assumption that we have a pre-trained neural network; Then, from a deterministic target image of size $M \times N$, for which we want to obtain a corrupt label, we define the prior knowledge on the input layer by the mean vector corresponding to the deterministic image $\boldsymbol{\mu}_X = \boldsymbol{x} \in \mathbb{R}^{M \times N}$, and a diagonal

covariance $\Sigma_{\mathbf{X}} = \sigma_X^2 \cdot \mathbf{I}$. Here, the amount of change that TAGI will apply on the original image during the inference procedure is controlled by the input layer’s standard deviation parameter σ_X . This prior knowledge about the target image is propagated forward through the network analogously to the procedure presented in §2. Then, when it is time to observe the label, the correct one is replaced by the target label \tilde{y} that is chosen for the attack. After performing the inference step, the initial image defined by its updated mean vector $\mu_{\mathbf{X}|\tilde{y}}$ and covariance $\Sigma_{\mathbf{X}|\tilde{y}}$ is now modified in order to trigger the class \tilde{y} . In order to improve the quality of the attack, the process is repeated recursively over multiple iterations, where the inferred values $\{\mu_{\mathbf{X}|\tilde{y}}^{(i)}, \Sigma_{\mathbf{X}|\tilde{y}}^{(i)}\}$ at iteration i are used as the prior’s hyper-parameters at the next iteration $i + 1$.

Figure 1 presents two examples where pre-trained convolutional neural networks [15] are employed to generate attacks for the images from a) the MNIST and b) the Cifar10 dataset. For all experiments, we set $\sigma_X = 0.03$ with a maximal number of epochs $\mathbf{E} = 100$. The networks’ details are presented in Appendix A.

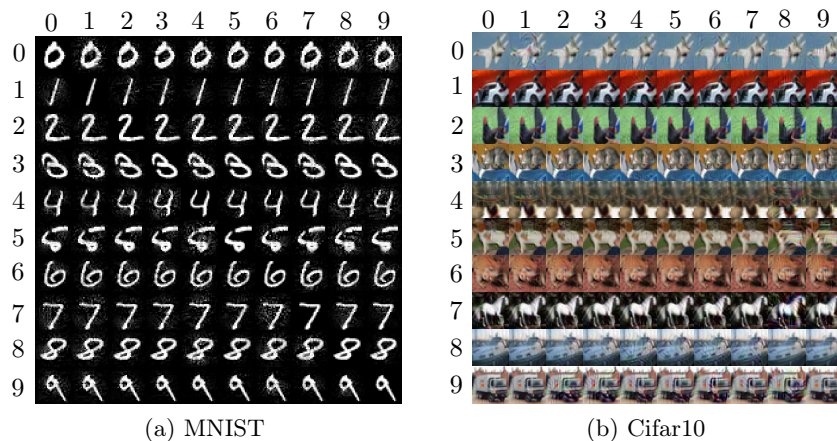


Figure 1: Examples of images subjected to adversarial attacks with different target labels \tilde{y} . Columns represent the different target labels \tilde{y} and rows are the true label images.

Table 1 compares the error rates obtained: without attack, with targeted attacks where a specific class is sought, and with non-targeted attacks where the goal is simply to fool the network. These results obtained for convolutional architectures confirm that TAGI can, without relying on an optimization

Table 1: Quantitative performance evaluation of TAGI’s adversarial attacks on MNIST and Cifar10.

Dataset	Model	Error Rate [%]		
		No attack	Targeted attack	Non-targeted attack
MNIST	2 conv.	0.64	99.8	99.9
Cifar10	3 conv.	22.0	99.6	99.9

scheme, infer adversarial-attack examples that are visually indistinguishable from the original.

4 Optimization through Inference

This section presents how we can leverage TAGI’s inference capabilities to find the local maxima or minima of a function. In general, a feedforward neural network (FNN) is a function approximation such that

$$y = g(\mathbf{x}; \boldsymbol{\theta}) + v, \tag{1}$$

where $\mathbf{x} \in \mathbb{R}^x$ is a vector of covariates, $y \in \mathbb{R}$ is the observed system response, $v \in \mathbb{R}$ is the observation error, and $\boldsymbol{\theta}$ is a vector of the parameters defining the weights \mathbf{w} and biases \mathbf{b} from the neural network $g(\mathbf{x}; \boldsymbol{\theta}) \in \mathbb{R}$. Figure 2 presents a compact representation for the directed acyclic graph (DAG) describing the dependency between the different components of such a FNN. The red node describes the input layer, green nodes either hidden or output layers, the purple node is an observed system response, and gray arrows represent the dependencies encoded in the parameters of the network. The red arrows represent the flow of information during the inference procedure described in §2, where TAGI infers the weights and biases of the network in a layer-wise fashion in order to maximize the computational and memory efficiency.

Once the parameters $\boldsymbol{\theta}$ of a neural network are learned, we can use the hidden units on the output layer $z^{(0)} = g(\mathbf{x}; \boldsymbol{\theta})$ to predict the responses associated with covariates \mathbf{x} , and we also have access to the n^{th} derivatives of the function approximation,

$$g^n(\mathbf{x}; \boldsymbol{\theta}) = \frac{\partial^n z^{(0)}}{\partial \mathbf{x}^n}. \tag{2}$$

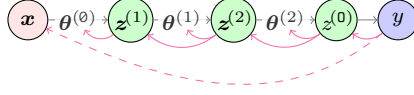


Figure 2: Compact representation of the variable nomenclature and the dependencies associated with a feedforward neural network with two hidden layers.

The details regarding the analytical calculation of partial derivatives using TAGI are presented in Appendix B. In the context of an optimization problem, the goal is to identify the input \mathbf{x} that maximizes or minimizes $z^{(0)}$, at which the first derivative of the function approximation is equal to zero, i.e., $g^1(\mathbf{x}; \boldsymbol{\theta}) = z'^{(0)} = 0$. Using the same inference procedure presented in §2, we can infer analytically the probability density function (PDF) $f(\mathbf{x}|z'^{(0)} = 0) = \mathcal{N}(\mathbf{x}; \boldsymbol{\mu}_{\mathbf{X}|z'}, \boldsymbol{\Sigma}_{\mathbf{X}|z'})$. For that purpose, we first define the prior knowledge for the vector of covariates \mathbf{x} so that $\mathbf{X} \sim \mathcal{N}(\mathbf{x}; \boldsymbol{\mu}_{\mathbf{X}}, \boldsymbol{\Sigma}_{\mathbf{X}})$. Then, the expected value $\boldsymbol{\mu}_{\mathbf{X}|z'}$ and variance $\boldsymbol{\Sigma}_{\mathbf{X}|z'}$ are computed following

$$\begin{aligned} \boldsymbol{\mu}_{\mathbf{X}|z'} &= \boldsymbol{\mu}_{\mathbf{X}} - \boldsymbol{\Sigma}_{Z'^{(0)}\mathbf{X}}^{\top} \left(\sigma_{Z'}^{(0)} \right)^{-2} \mu_{Z'}^{(0)} \\ \boldsymbol{\Sigma}_{\mathbf{X}|z'} &= \boldsymbol{\Sigma}_{\mathbf{X}} - \boldsymbol{\Sigma}_{Z'^{(0)}\mathbf{X}}^{\top} \left(\sigma_{Z'}^{(0)} \right)^{-2} \boldsymbol{\Sigma}_{Z'^{(0)}\mathbf{X}}, \end{aligned} \quad (3)$$

where the expected value $\mathbb{E}[Z'^{(0)}] = \mu_{Z'}^{(0)}$, variance $\text{var}[Z'^{(0)}] = (\sigma_{Z'}^{(0)})^2$, and covariance $\boldsymbol{\Sigma}_{Z'^{(0)}\mathbf{X}} = \text{cov}(Z'^{(0)}, \mathbf{X})$ are obtained using the forward propagation of uncertainty defined for TAGI. In order to ensure that the inferred values for \mathbf{x} correspond to either a minimum or a maximum, we need to rely the sign of the first derivative to control the direction of the mean update step. The expected value in Equation 3 is thus reformulated as

$$\boldsymbol{\mu}_{\mathbf{X}|z'} = \boldsymbol{\mu}_{\mathbf{X}} + \alpha \cdot \text{sign}\left(\frac{\partial z'^{(0)}}{\partial \mathbf{x}}\right) \left| \boldsymbol{\Sigma}_{\mathbf{0}\mathbf{X}}^{\top} \left(\sigma_{Z'}^{(0)} \right)^{-2} \mu_{Z'}^{(0)} \right|, \quad (4)$$

where $\alpha = 1$ when seeking a maximum, and -1 for a minimum.

In order to seek the location where the derivative is equal to zero, we repeat the inference multiple times where the inferred values $\{\boldsymbol{\mu}_{\mathbf{X}|z'}^{(i)}, \boldsymbol{\Sigma}_{\mathbf{X}|z'}^{(i)}\}$ at iteration i are used as the prior's hyper-parameters at the next iteration $i + 1$. The algorithm 1 presents an example of the implementation for the optimization of a function using TAGI's inference capacity.

We illustrate the inference-based optimization scheme on a 1D toy problem for $y = x^3 - 3x + v$ as depicted in Figure 3a, where the observation errors $V \sim$

Algorithm 1: Optimization of a function using TAGI

```
1 Define a neural network  $g(\mathbf{x}; \boldsymbol{\theta})$ ;  
2 Initialize  $\sigma_V$ , the prior for  $\boldsymbol{\theta}$  and for the covariates  $\mathbf{X}$ ;  
3 Given a dataset  $\mathcal{D} = \{\mathbf{x}_i, y_i\}, \forall i = \{1, 2, \dots, D\}$ ;  
4 for  $epoch = 1 : E$  do  
5   for  $i = 1 : D$  do  
6     Compute the prediction for a given input  $\mathbf{x}_i$ ;  
7      $\{\mu_Y, \sigma_Y^2\} = g(\mathbf{x}_i; \boldsymbol{\theta})$ ;  
8     Update  $\boldsymbol{\mu}_{\boldsymbol{\theta}|\mathcal{D}}, \boldsymbol{\Sigma}_{\boldsymbol{\theta}|\mathcal{D}}$  using TAGI;  
9     Compute the partial derivative of  $g(\mathbf{x}; \boldsymbol{\theta})$  w.r.t.  $\mathbf{x}$ ;  
10    Update  $\boldsymbol{\mu}_{\mathbf{X}|z'}, \boldsymbol{\Sigma}_{\mathbf{X}|z'}$  using Equation 4;
```

$\mathcal{N}(0, 0.1^2)$. The function approximation obtained using TAGI is presented in Figure 3b and its derivative in Figure 3c. We use this toy problem to illustrate how we use the derivative constraint α in order to reach either the local maximum at $x = -1$ or the local minimum at $x = +1$.

Table 2 presents the optimal location $\mu_{X|z'}$ found by TAGI depending on the starting location μ_X^θ and whether or not a derivative constraint α is employed. Note that for all cases, the initial input variance is set to $\sigma_X = 0.01$. The results show that when no derivative constraint α is employed, the optimal value reached correspond to either a maximum or a minimum, depending on the starting location μ_X^θ . More specifically, the inference will lead to the maximum or minimum associated within the region where the sign of the covariance is the same as for the starting location μ_X^θ , as depicted in Figure 3d. A positive derivative constrain α leads to the local minimum whether starting in a region having a positive or negative covariance. On the other hand, a negative constrain leads to the local maximum. Note that whether or not we use a derivative constrain α , TAGI will fail to infer the local maximum at $x = -1$ while starting at a value such as $x = 1.9$, because the sign of the covariance estimated using TAGI is incorrect so that the optimal location inferred will be pushed beyond the value $x = +2$. This example illustrates a limitation of TAGI's inference-based optimization scheme where, like for gradient-based approaches, the starting location μ_X^θ matters.

Although this optimization problem is trivial as it involves only one dimension, it showcases how the inference capability of TAGI can be leveraged

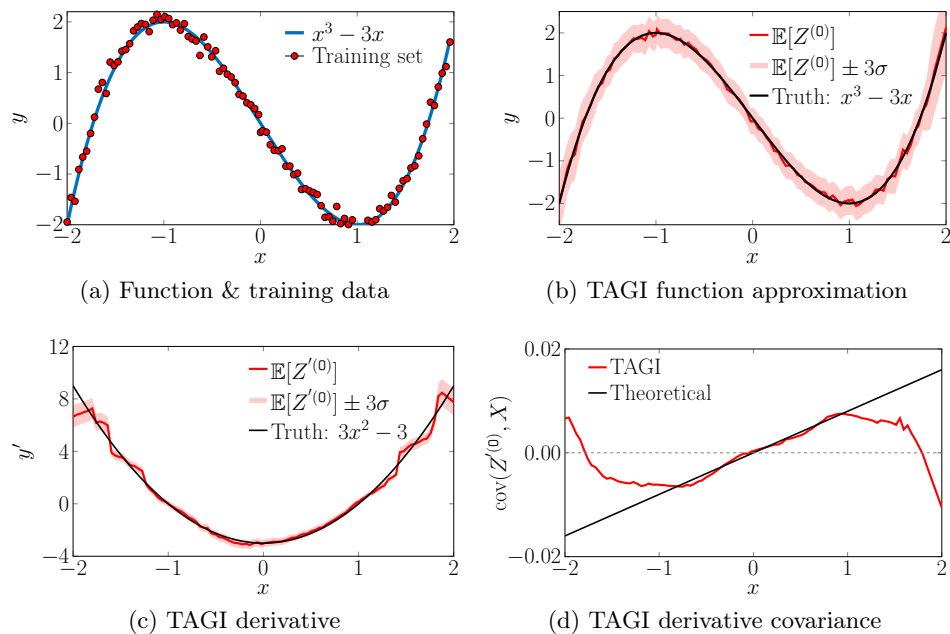


Figure 3: 1D optimization problem

Table 2: Comparison of the optimal values obtained $\mu_{X|z'}$ depending on the starting location μ_X° and whether or not a derivative constraint α is employed.

μ_X°	α	Update equation	$\mu_{X z'}$
0.25	N/A	Eq. 3	0.965
-0.25	N/A	Eq. 3	-0.992
0.25	+1	Eq. 4	-0.993
-0.25	+1	Eq. 4	-0.992
0.25	-1	Eq. 4	0.965
-0.25	-1	Eq. 4	0.965

in order to solve optimization tasks. The next section will build on that capacity in order to tackle continuous-actions reinforcement learning problems which involve optimization in higher-dimensional spaces.

5 Continuous-Actions RL through Inference

This section presents how to perform continuous-actions reinforcement learning (RL) by leveraging hidden-state inference. For both categorical and continuous actions RL frameworks, an agent’s goal is to maximize the expected value conditional on an action a . For categorical actions, this can be achieved through the explicit evaluation of the expected value for each action and the selection of the optimal one. In the case of continuous actions, it is not possible nor desirable to evaluate the expected value associated with all possible actions; one thus face a continuous optimization problem. In deep-RL methods such as advantage actor critic (A2C) [13] and proximal policy optimization (PPO) [17], this optimization is tackled using gradient ascent approaches. Here, we rely instead on the method presented in §4 to identify the optimal action through inference.

For typical RL problems, the environment’s state at a time t and $t + 1$ are $\{\mathbf{s}, \mathbf{s}'\} \in \mathbb{R}^{\mathbb{N}^2}$, and the expected utility conditional on the actions $\mathbf{a} \in \mathbb{R}^{\mathbb{A}}$ and states \mathbf{s} is defined by the action-value function $q(\mathbf{s}, \mathbf{a}) \in \mathbb{R}^1$. Figure 4a presents the directed acyclic graph (DAG) describing the interconnectivity in a neural network capable of modelling a policy network, i.e., the dependency between the actions \mathbf{a} and the states \mathbf{s} . Figure 4b presents a similar graph for a value network modelling the dependency between the action-value function q , and the actions \mathbf{a} and states \mathbf{s} . Figure 4c presents the combination of the value and policy networks from (a) and (b) in a single network that is analogous to the temporal-difference learning framework by Nguyen and Goulet [14], where $\{\mathbf{s}, \mathbf{a}\}$ are the states and action at a time t and $\{\mathbf{s}', \mathbf{a}'\}$ the states and action at a time $t + 1$. In this graph, the nodes that have been doubled represent the states \mathbf{s} and \mathbf{s}' which are both evaluated in a network sharing the same parameters in order to learn from the observation equation

$$q(\mathbf{s}, \mathbf{a}) = r(\mathbf{s}) + \gamma q(\mathbf{s}', \mathbf{a}') + \sigma_V \epsilon, \quad (5)$$

where ϵ is a realization from a standard-normal random variable, $r(\mathbf{s})$ is the reward function, and γ is the discount factor.

One particularity in the graph from Figure 4c is that the actions $\{\mathbf{a}, \mathbf{a}'\}$ are deterministic inputs (red nodes), as the specific actions at a time t are sampled from their current posterior predictive distribution. The red

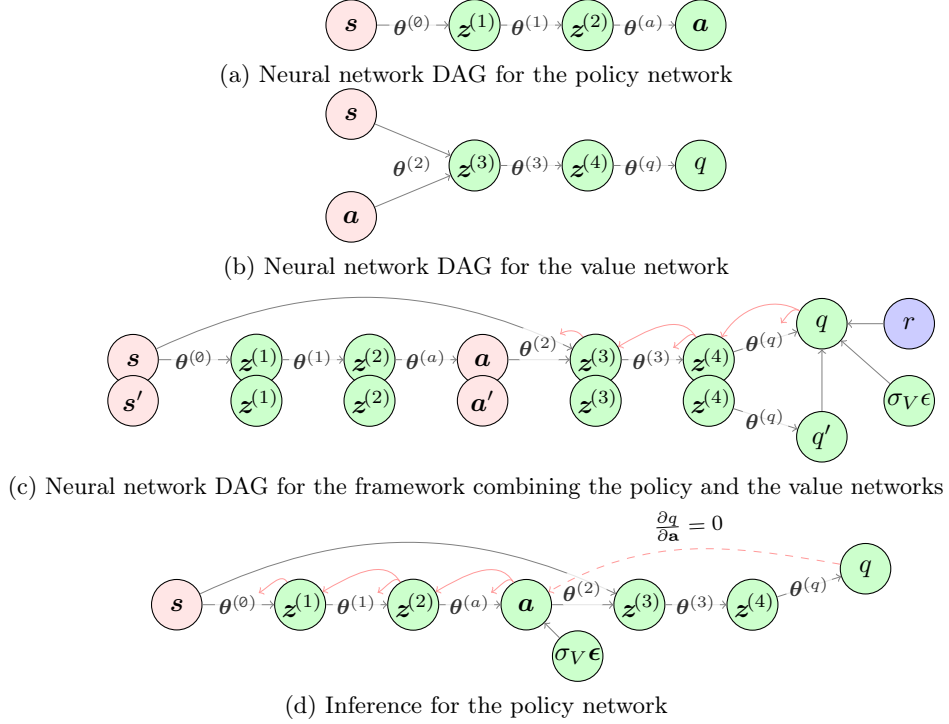


Figure 4: Graphical representation of a neural network structure for temporal-difference Q-policy learning for continuous actions.

arrows outline the flow of information during the inference procedure for the components belonging to the value network. Note that the policy network cannot be updated directly because the flow of information in Figure 4c is broken by the knowledge of the actions. The component belonging to the policy network are thus updated separately as depicted in Figure 4d, where the prior for the actions \mathbf{a} is computed from the policy network so that

$$\mathbf{a} = \mathbf{w}^{(a)} \mathbf{z}^{(2)} + \mathbf{b}^{(a)} + \sigma_V \epsilon, \quad (6)$$

and where the inference for the actions uses the constrain on the derivative

$$\mathbf{a} : \frac{\partial q}{\partial \mathbf{a}} = 0. \quad (7)$$

Algorithm 2 details an example of implementation for the on-policy reinforcement learning in the context of TAGI.

We compare the performance of this on-policy TD reinforcement learning framework for continuous actions with the PPO method [17]. We perform

Algorithm 2: Continuous-action reinforcement learning with TAGI

```
1 Define policy network  $\mathcal{P}(\mathbf{s}; \boldsymbol{\theta}^{\mathcal{P}})$ , value network  $\mathcal{Q}(\mathbf{s}, \mathbf{a}; \boldsymbol{\theta}^{\mathcal{Q}})$ ;
2 Initialize  $\boldsymbol{\theta}^{\mathcal{P}}$ ,  $\boldsymbol{\theta}^{\mathcal{Q}}$ ,  $\sigma_V$ , horizon  $H$ , memory  $\mathcal{R}$  to capacity  $H$ 
3 steps = 0;
4 for episode = 1 :  $E$  do
5   Reset environment  $\mathbf{s}_1$ ;
6   for  $t = 1 : T$  do
7     steps = steps + 1;
8      $\{\boldsymbol{\mu}_t^{\mathbf{A}}, \boldsymbol{\Sigma}_t^{\mathbf{A}}\} = \mathcal{P}(\mathbf{s}_t; \boldsymbol{\theta}^{\mathcal{P}})$ ;
9      $\mathbf{a}_t : \mathbf{A}_t \sim \mathcal{N}(\boldsymbol{\mu}_t^{\mathbf{A}}, \boldsymbol{\Sigma}_t^{\mathbf{A}})$ ;
10     $\mathbf{s}_{t+1}, r_t = \text{environment}(\mathbf{a}_t)$ ;
11    Store  $\{\mathbf{s}_t, \mathbf{a}_t, r_t\}$  in  $\mathcal{R}$ ;
12    if steps mod H == 0 then
13       $\{\boldsymbol{\mu}_{t+1}^{\mathbf{A}}, \boldsymbol{\Sigma}_{t+1}^{\mathbf{A}}\} = \mathcal{P}(\mathbf{s}_{t+1}; \boldsymbol{\theta}^{\mathcal{P}})$ ;
14       $\mathbf{a}_{t+1} : \mathbf{A}_{t+1} \sim \mathcal{N}(\boldsymbol{\mu}_{t+1}^{\mathbf{A}}, \boldsymbol{\Sigma}_{t+1}^{\mathbf{A}})$ ;
15       $\{\boldsymbol{\mu}_{t+1}^{\mathcal{Q}}, (\sigma_{t+1}^{\mathcal{Q}})^2\} = \mathcal{Q}(\mathbf{s}_{t+1}, \mathbf{a}_{t+1}; \boldsymbol{\theta}^{\mathcal{Q}})$ ;
16      Take  $H$  samples of  $\{\mathbf{s}, \mathbf{a}, r\}$  from  $\mathcal{R}$ ;
17       $\mu_{\mathbf{H}}^{\mathbf{Y}} = \mu_{t+1}^{\mathcal{Q}}; \sigma_{\mathbf{H}}^{\mathbf{Y}} = \sigma_{t+1}^{\mathcal{Q}}$ ;
18      for  $j = H - 1 : 1$  do
19         $\mu_j^{\mathbf{Y}} = r_j + \gamma \mu_{j+1}^{\mathbf{Y}}; (\sigma_j^{\mathbf{Y}})^2 = \gamma^2 (\sigma_{j+1}^{\mathbf{Y}})^2 + \sigma_V^2$ ;
20      Update  $\boldsymbol{\theta}^{\mathcal{Q}}$  using TAGI;
21      Update  $\boldsymbol{\theta}^{\mathcal{P}}$  using TAGI and Algorithm 1 with the
        constraint  $\frac{\partial q}{\partial \mathbf{a}} = 0$ ;
22      Initialize memory  $\mathcal{R}$  to capacity  $H$ ;
```

this comparison on the half-cheetah and inverted pendulum problems from the Mujoco environment [19] implemented in OpenAI Gym [3]. For the TAGI-based approach, the Q-value network uses a FNN with three hidden layers of 128 units. The policy network employs a FNN with two hidden layers of 128 units. The standard deviation σ_V in Equation 5 and 6 is initialized at 2 and is decayed each 1024 steps with a decaying factor of 0.9999. The minimal standard deviation is $\sigma_V^{\min} = 0.3$. These hyperparameters are kept constant for both environments. For the PPO approach, we use the same model architecture for both the policy and value networks as well as the hyper-parameter values from Open AI baselines [5]. During training, the TAGI-based approach uses a single epoch while PPO employs ten. The details for the model architecture and hyper-parameter values are provided in Appendix A.3. Figure 5 shows the average reward over 100 episodes with respect to the number of steps for both environments. Table 3 presents the

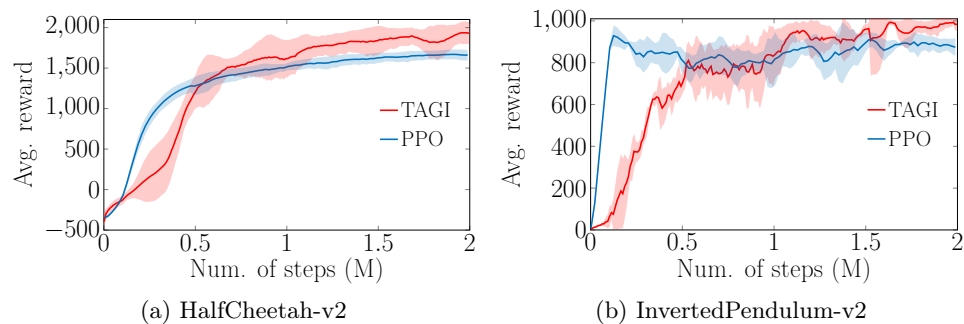


Figure 5: Illustration of average reward over 100 episodes of five random runs for two millions time steps.

average reward over the last 100 episodes for both environments. Although PPO initially learns faster, the final results show that TAGI outperforms PPO on both experiments. In addition, TAGI requires fewer hyper-parameters than PPO (see Table 9 in Appendix A.3). Note that the goal of this experiment is to demonstrate how can inference be leveraged for solving existing problems with a novel approach. The application of TAGI to RL problems is in its early days and it is foreseeable that if more time is invested in exploring new architectures and network configurations, the framework could further exceed the current performance.

Table 3: Average reward over the last 100 episodes of five random runs for the half-cheetah and inverted pendulum experiments. TAGI: Tractable Approximate Gaussian Inference; PPO: Proximal Policy Optimization.

Method	Half-cheetah	Inverted pendulum
TAGI	1934 ± 131	983 ± 30
PPO	1649 ± 48	887 ± 42

6 Conclusion

TAGI provides a novel capacity to perform inference in neural networks. Its applications to adversarial attacks, optimization, and continuous-action reinforcement learning showcase how these tasks, which previously relied on gradient-based optimization methods, can now be approached with analytically tractable inference. The applications presented in this paper are only a subset from the variety of problems that can take advantage of inference, either through the adaptation of existing architectures or through the development of new ones.

Acknowledgements

The first author was financially supported by research grants from Hydro-Quebec, and the Natural Sciences and Engineering Research Council of Canada (NSERC). We would like to thank Magali Goulet and Prof. Mélina Mailhot for having reviewed the equations employed for computing the derivatives.

References

- [1] N. Akhtar and A. Mian. Threat of adversarial attacks on deep learning in computer vision: A survey. *IEEE Access*, 6:14410–14430, 2018.
- [2] L. Ardizzone, J. Kruse, C. Rother, and U. Köthe. Analyzing inverse problems with invertible neural networks. In *International Conference on Learning Representations*, 2019.

- [3] G. Brockman, V. Cheung, L. Pettersson, J. Schneider, J. Schulman, J. Tang, and W. Zaremba. Openai gym. *arXiv preprint arXiv:1606.01540*, 2016.
- [4] X. Chen, Y. Duan, R. Houthoofd, J. Schulman, I. Sutskever, and P. Abbeel. Infogan: Interpretable representation learning by information maximizing generative adversarial nets. *arXiv:1606.03657*, 2016.
- [5] P. Dhariwal, C. Hesse, O. Klimov, A. Nichol, M. Plappert, A. Radford, J. Schulman, S. Sidor, Y. Wu, and P. Zhokhov. Openai baselines. <https://github.com/openai/baselines>, 2017.
- [6] I. Goodfellow, Y. Bengio, and A. Courville. *Deep learning*. MIT Press, 2016.
- [7] I. Goodfellow, J. Pouget-Abadie, M. Mirza, B. Xu, D. Warde-Farley, S. Ozair, A. Courville, and Y. Bengio. Generative adversarial nets. *Advances in neural information processing systems*, 27:2672–2680, 2014.
- [8] I. Goodfellow, J. Shlens, and C. Szegedy. Explaining and harnessing adversarial examples. In *International Conference on Learning Representations*, 2015.
- [9] J.-A. Goulet, L. Nguyen, and S. Amiri. Tractable approximate Gaussian inference for Bayesian neural networks. *arXiv preprint*, 2020.
- [10] J.-A. Goulet, L. H. Nguyen, and S. Amiri. Tractable approximate gaussian inference for Bayesian neural networks. *arXiv*, (2004.09281, cs.LG), 2020.
- [11] D. P. Kingma and M. Welling. Auto-encoding variational Bayes. *arXiv preprint arXiv:1312.6114*, 2013.
- [12] J. Kruse, L. Ardizzone, C. Rother, and U. Köthe. Benchmarking invertible architectures on inverse problems, 2021.
- [13] V. Mnih, A. P. Badia, M. Mirza, A. Graves, T. Lillicrap, T. Harley, D. Silver, and K. Kavukcuoglu. Asynchronous methods for deep reinforcement learning. In *International conference on machine learning*, pages 1928–1937. PMLR, 2016.
- [14] L. H. Nguyen and J.-A. Goulet. Analytically tractable Bayesian deep Q-learning. *arXiv preprint arXiv:2106.11086*, 2021.

- [15] L. H. Nguyen and J.-A. Goulet. Analytically tractable inference in deep neural networks. *arXiv preprint arXiv:2103.05461*, 2021.
- [16] D. E. Rumelhart, G. E. Hinton, and R. J. Williams. Learning representations by back-propagating errors. *Nature*, 323:533—536, 1986.
- [17] J. Schulman, F. Wolski, P. Dhariwal, A. Radford, and O. Klimov. Proximal policy optimization algorithms. *arXiv preprint arXiv:1707.06347*, 2017.
- [18] R. S. Sutton and A. G. Barto. *Reinforcement learning: An introduction*. MIT Press, 2nd edition, 2018.
- [19] E. Todorov, T. Erez, and Y. Tassa. Mujoco: A physics engine for model-based control. In *2012 IEEE/RSJ International Conference on Intelligent Robots and Systems*, pages 5026–5033. IEEE, 2012.

A Model Architecture and Hyper-parameters

This appendix contains the specifications for each model architecture in the experiment section. D refers to a layer depth; W refers to a layer width; H refers to the layer height in case of convolutional or pooling layers; K refers to the kernel size; P refers to the convolutional kernel padding; S refers to the convolution stride; ϕ refers to the activation function type; ReLU refers to rectified linear unit;

A.1 Adversarial Attack

A.1.1 MNIST

Table 4: Configuration details for the CNN applied to the MNIST adversarial attack.

Layer	$D \times W \times H$	$K \times K$	P	S	ϕ
Input	$1 \times 28 \times 28$	-	-	-	-
Convolutional	$32 \times 27 \times 27$	4×4	1	1	ReLU
Pooling	$32 \times 13 \times 13$	3×3	0	2	-
Convolutional	$64 \times 9 \times 9$	5×5	0	1	ReLU
Pooling	$64 \times 4 \times 4$	3×3	0	2	-
Fully connected	$150 \times 1 \times 1$	-	-	-	ReLU
Output	$11 \times 1 \times 1$	-	-	-	-

A.1.2 Cifar10

Table 5: Configuration details for the CNN applied to the Cifar10 adversarial attack

Layer	$D \times W \times H$	$K \times K$	P	S	ϕ
Input	$3 \times 32 \times 32$	-	-	-	-
Convolutional	$32 \times 32 \times 32$	5×5	2	1	ReLU
Pooling	$32 \times 16 \times 16$	3×3	1	2	-
Convolutional	$32 \times 16 \times 16$	5×5	2	1	ReLU
Average pooling	$32 \times 8 \times 8$	3×3	1	2	-
Convolutional	$64 \times 8 \times 8$	5×5	2	1	ReLU
Average pooling	$64 \times 4 \times 4$	3×3	1	2	-
Fully connected	$64 \times 1 \times 1$	-	-	-	ReLU
Output	$11 \times 1 \times 1$	-	-	-	-

A.2 Optimization

Table 6: Configuration details for the feedforward neural network applied to 1D example.

Layer	$D \times W \times H$	$K \times K$	P	S	ϕ
Input	$1 \times 1 \times 1$	-	-	-	-
Fully connected	$64 \times 1 \times 1$	-	-	-	Tanh
Fully connected	$64 \times 1 \times 1$	-	-	-	ReLU
Output	$1 \times 1 \times 1$	-	-	-	-

A.3 Continuous-Action Reinforcement Learning

For the half-cheatah environment, the number of states N_s is 17 and the number of actions N_a is 6. For the inverted pendulum environment, the number of states N_s is 4 and the number of actions N_a is 1.

Table 7: Configuration details for the policy network. N_s is the number of states; N_a is the number of actions.

Layer	$D \times W \times H$	$K \times K$	P	S	ϕ
Input	$N_s \times 1 \times 1$	-	-	-	-
Fully connected	$128 \times 1 \times 1$	-	-	-	ReLU
Fully connected	$128 \times 1 \times 1$	-	-	-	ReLU
Output	$N_a \times 1 \times 1$	-	-	-	Tanh

Table 8: Configuration details for the Q-value network. N_s is the number of states.

Layer	$D \times W \times H$	$K \times K$	P	S	ϕ
Input	$N_s \times 1 \times 1$	-	-	-	-
Fully connected	$128 \times 1 \times 1$	-	-	-	Tanh
Fully connected	$128 \times 1 \times 1$	-	-	-	ReLU
Fully connected	$128 \times 1 \times 1$	-	-	-	ReLU
Output	$1 \times 1 \times 1$	-	-	-	-

Table 9: Hyper-parameters for half-cheetah and inverted pendulum problems.

Method	#	Hyperparameter	Value
TAGI	1	Horizon	1024
	2	Initial standard deviation for the value function (σ_V)	2
	3	Decay factor (η)	0.9999
	4	Minimal standard deviation for the value function (σ_V^{\min})	0.3
	5	Batch size	16
	6	Number of epochs	1
	7	Discount (γ)	0.99
PPO	1	Horizon	2048
	2	Adam stepsize	$3 \times 10^{-4} \times \alpha$
	3	Adam epsilon	10^{-5}
	4	Adam β_1	0.9
	5	Adam β_2	0.999
	6	Batch size	32
	7	Number of epochs	10
	8	Discount (γ)	0.99
	9	Generalized advantage estimation parameter (λ)	0.95
	10	Clipping parameter (ϵ)	$0.2 \times \alpha$
	11	Value function loss coefficient (c_1)	1
	12	Entropy coefficient (c_2)	0.0
	13	Gradient norm clipping coefficient	0.5
	14	α	LinearAnneal(1, 0)

B Partial Derivative in TAGI Neural Networks

B.1 TAGI Neural Networks

In a feedforward neural network, the hidden state at a given layer $l + 1$ is defined as

$$Z_i^{(l+1)} = \sum_k W_{ik}^{(l)} \phi(Z_k^{(l)}) + B_i^{(l)}, \quad \forall i \in [1, \mathbf{A}^{(l+1)}], \forall k \in [1, \mathbf{A}^{(l)}], \forall l \in [1, \mathbf{L}] \quad (8)$$

where $\phi(\cdot)$ is the activation function, $\{W, B\}$ are the unknown parameters of the neural network, i.e. weight and bias, $\mathbf{A}^{(l)}$, is the number of hidden units in layer l and \mathbf{L} is the number of hidden layers. We define the activation unit $A = \phi(Z)$. In the context of TAGI, Z, W , and B are assumed to be Gaussian random variables and

$$\begin{aligned} W_{ik}^{(l)} &\perp\!\!\!\perp W_{np}^{(m)} \perp\!\!\!\perp B_i^{(l)} \perp\!\!\!\perp B_n^{(m)}, \quad \forall m \in [1, \mathbf{L}], \forall n \in [1, \mathbf{A}^{(m+1)}], \forall p \in [1, \mathbf{A}^{(m)}] \\ Z_t^{(l-1)} &\perp\!\!\!\perp Z_i^{(l+1)}, \quad \forall t \in [1, \mathbf{A}^{(l-1)}] \\ Z_k^{(l)} &\perp\!\!\!\perp Z_q^{(l)}, \quad \forall q \in [1, \mathbf{A}^{(l)}] \text{ and } k \neq q \\ Z_k^{(l)} &\perp\!\!\!\perp W_{ik}^{(l)} \perp\!\!\!\perp B_i^{(l)}. \end{aligned} \quad (9)$$

In addition, we apply the locally linearized activation function $\tilde{\phi}(\cdot)$ to the hidden state in order to obtain the probability density function for the output of $\phi(\cdot)$ so that

$$\phi(Z_k^{(l)}) = J_k^{(l)} \left(Z_k^{(l)} - \mathbb{E} \left[Z_k^{(l)} \right] \right) + \phi \left(\mathbb{E} \left[Z_k^{(l)} \right] \right), \quad (10)$$

where $J_k^{(l)} = \nabla_z \phi \left(\mathbb{E} \left[Z_k^{(l)} \right] \right)$.

B.2 Gaussian Multiplication Approximation (GMA)

Assuming $\mathbf{X} = [X_1 \dots X_4]^\top$ are Gaussian random variables, the GMA formulation had been defined by Goulet, Nguyen and Amiri [10] as

$$\mathbb{E}[X_1 X_2] = \mu_1 \mu_2 + \text{cov}(X_1, X_2), \quad (11)$$

$$\text{cov}(X_3, X_1 X_2) = \text{cov}(X_1, X_3) \mu_2 + \text{cov}(X_2, X_3) \mu_1, \quad (12)$$

$$\begin{aligned} \text{cov}(X_1 X_2, X_3 X_4) &= \text{cov}(X_1, X_3) \text{cov}(X_2, X_4) \\ &\quad + \text{cov}(X_1, X_4) \text{cov}(X_2, X_3) \end{aligned} \quad (13)$$

$$\begin{aligned} &\quad + \text{cov}(X_1, X_3) \mu_2 \mu_4 + \text{cov}(X_1, X_4) \mu_2 \mu_3 \\ &\quad + \text{cov}(X_2, X_3) \mu_1 \mu_4 + \text{cov}(X_2, X_4) \mu_1 \mu_3, \\ \text{var}(X_1 X_2) &= \sigma_1^2 \sigma_2^2 + \text{cov}(X_1, X_2)^2 \\ &\quad + 2 \text{cov}(X_1, X_2) \mu_1 \mu_2 + \sigma_1^2 \mu_2^2 + \sigma_2^2 \mu_1^2. \end{aligned} \quad (14)$$

B.3 Partial Derivative Formulations for A Simple Feedforward Neural Network

This section presents the partial derivative formulations for a feedforward neural network (FNN) of four layers in the context of TAGI. Figure 6 presents the details of the interconnectivity of the variables associated with a four-layer FNN, Figure 7 describes the partial derivative diagram for the four-layer FNN presented in Figure 6, and Figure 8 shows the partial derivative diagram associated with the parameters and hidden states. The partial derivative diagram allow computing the partial derivative of either a hidden state or an activation unit at any layers with respect to either the hidden state or activation unit from the previous layers. For example, the partial derivative of the first activation unit of layer three, i.e., $A_1^{(3)}$ with respect to the first hidden state of layer one, i.e., $Z_1^{(1)}$ is the sum of the product of the partial derivatives of two branches relating to this partial derivative, which are identified using the partial derivative diagram in Figure 8. Figure 9 illustrates the computations of this partial derivative.

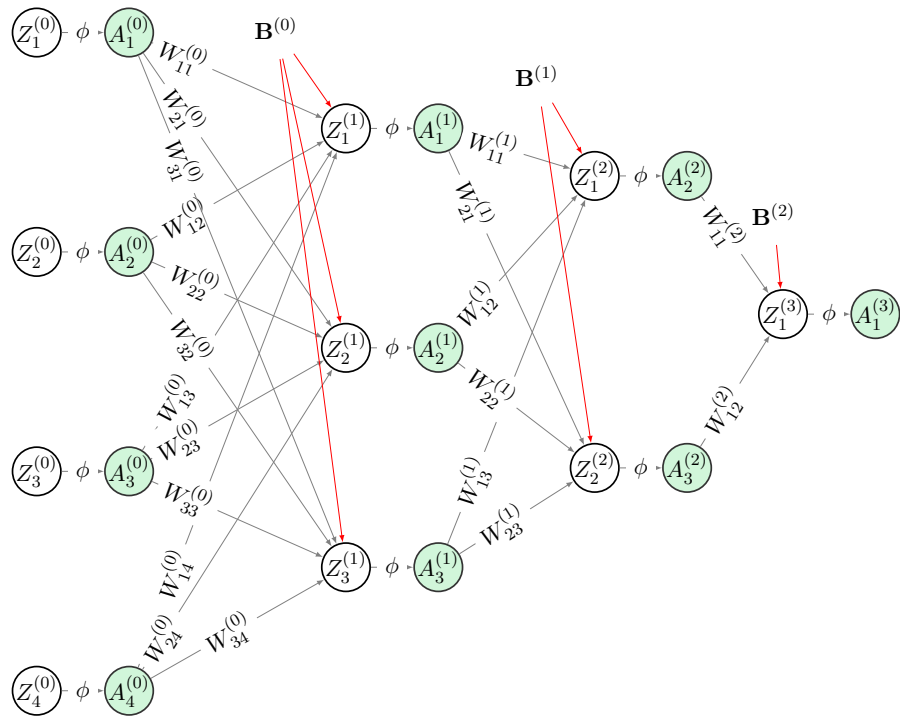


Figure 6: Illustration of parameters $\theta = \{\mathbf{W}, \mathbf{B}\}$, hidden states \mathbf{Z} , and activation units \mathbf{A} associated with a four-layer feedforward neural network.

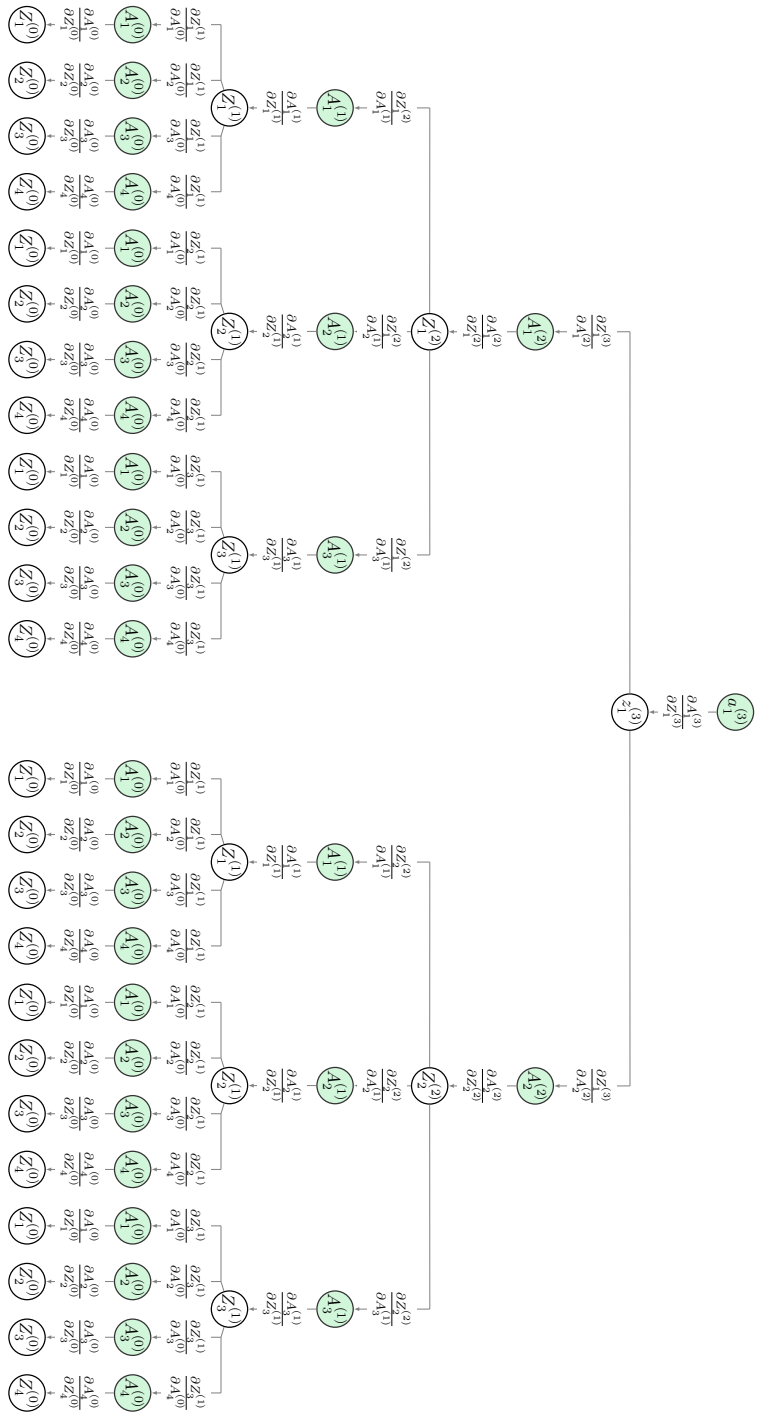
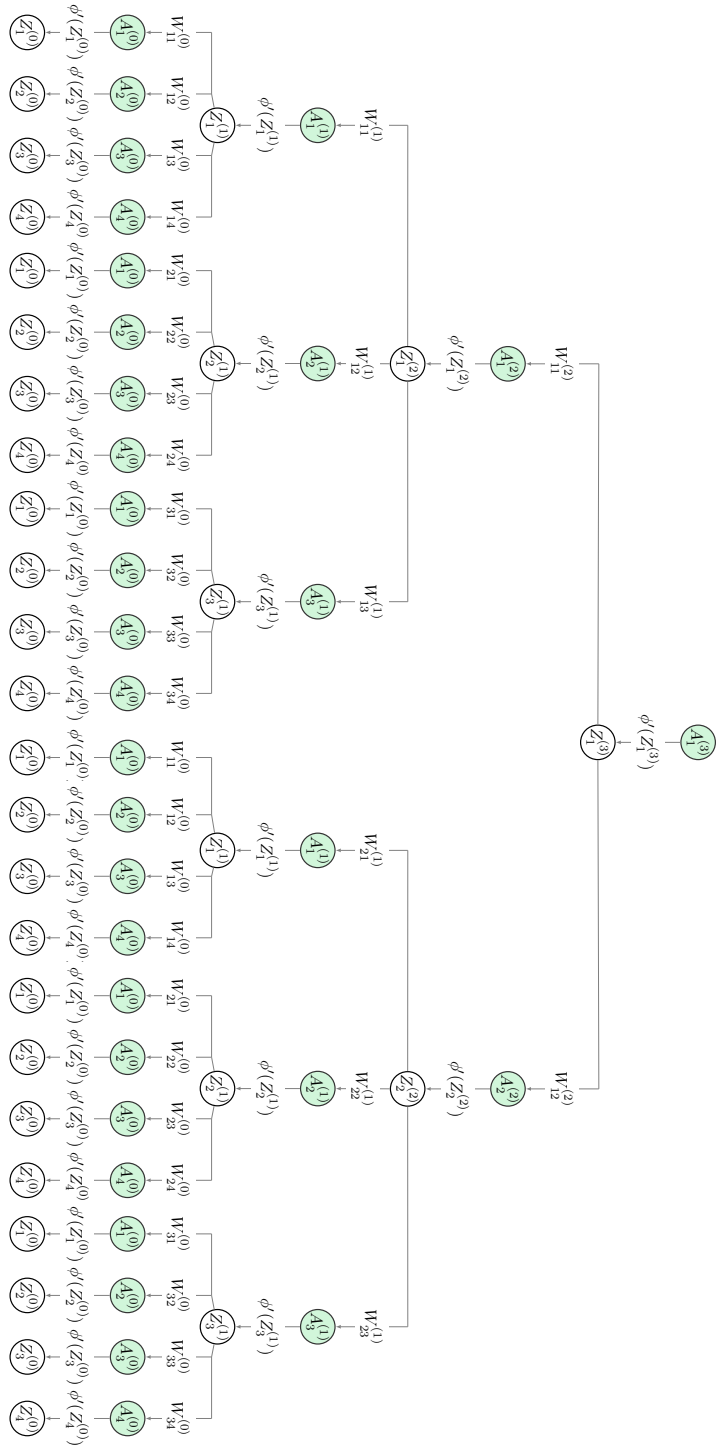


Figure 7: Illustration of partial derivative diagram for a four-layer feedforward neural network.



24
 Figure 8: Illustration of partial derivative diagram associated with the parameters and hidden states for a four-layer feedforward neural network.

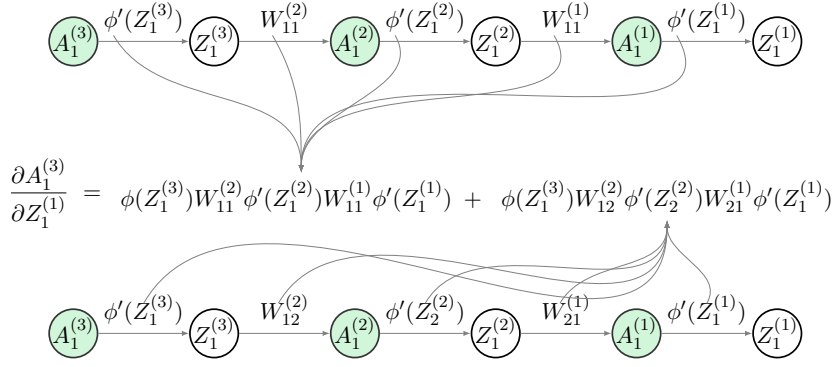


Figure 9: Illustration of the partial derivative of $A_1^{(3)}$ with respect to $Z_1^{(1)}$.

B.3.1 Partial Derivative $\frac{\partial A_1^{(3)}}{\partial Z_1^{(2)}}$

This section presents the calculations of the partial derivative of $A_1^{(3)}$ with respect to $Z_1^{(2)}$. Figure 10 shows the branch from the partial derivative diagram (Figure 8), that corresponds to this partial derivative. This partial

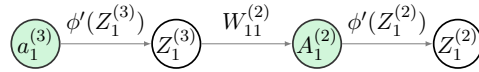


Figure 10: Illustration of a branch of the partial derivative of $A_1^{(3)}$ with respect to $Z_1^{(2)}$.

derivative is defined as

$$\frac{\partial A_1^{(3)}}{\partial Z_1^{(2)}} = \phi'(Z_1^{(3)})W_{11}^{(2)}\phi'(Z_1^{(2)}). \quad (15)$$

In the context of TAGI, the weights W and hidden states Z are Gaussian random variables, therefore, $\frac{\partial A_1^{(3)}}{\partial Z_1^{(2)}}$ is also approximated by a Gaussian PDF.

The expected value is computed using Equation 11 and 9,

$$\begin{aligned}\mathbb{E}\left[\frac{\partial A_1^{(3)}}{\partial Z_1^{(2)}}\right] &= \mathbb{E}\left[\phi'(Z_1^{(3)})W_{11}^{(2)}\phi'(Z_1^{(2)})\right] \\ &= \mathbb{E}\left[\phi'(Z_1^{(3)})\right]\mathbb{E}\left[W_{11}^{(2)}\phi'(Z_1^{(2)})\right] + \text{cov}\left(\phi'(Z_1^{(3)}), W_{11}^{(2)}\phi'(Z_1^{(2)})\right),\end{aligned}\tag{16}$$

where

$$\mathbb{E}\left[W_{11}^{(2)}\phi'(Z_1^{(2)})\right] = \mathbb{E}\left[W_{11}^{(2)}\right]\mathbb{E}\left[\phi'(Z_1^{(2)})\right] + \underbrace{\text{cov}\left(W_{11}^{(2)}, \phi'(Z_1^{(2)})\right)}_{\text{Eq. 9}}. \tag{17}$$

$$\begin{aligned}\text{cov}\left(\phi'(Z_1^{(3)}), W_{11}^{(2)}\phi'(Z_1^{(2)})\right) &= \text{cov}\left(\phi'(Z_1^{(3)}), W_{11}^{(2)}\right)\mathbb{E}\left[\phi'(Z_1^{(2)})\right] \\ &\quad + \text{cov}\left(\phi'(Z_1^{(3)}), \phi'(Z_1^{(2)})\right)\mathbb{E}\left[W_{11}^{(2)}\right].\end{aligned}\tag{18}$$

Note that the computations for the covariance $\text{cov}\left(\phi'(Z_1^{(3)}), W_{11}^{(2)}\right)$ and $\text{cov}\left(\phi'(Z_1^{(3)}), \phi'(Z_1^{(2)})\right)$ depend on the type of the activation function $\phi(\cdot)$ being used for this layer (see §B.5). The variance is computed using Equation 14, 9, 17, and 16,

$$\begin{aligned}\text{var}\left(\phi'(Z_1^{(3)})W_{11}^{(2)}\phi'(Z_1^{(2)})\right) &= \text{var}\left(\phi'(Z_1^{(3)})\right)\text{var}\left(W_{11}^{(2)}\phi'(Z_1^{(2)})\right) \\ &\quad + \text{cov}\left(\phi'(Z_1^{(3)}), W_{11}^{(2)}\phi'(Z_1^{(2)})\right)^2 \\ &\quad + 2\text{cov}\left(\phi'(Z_1^{(3)}), W_{11}^{(2)}\phi'(Z_1^{(2)})\right) \\ &\quad \times \mathbb{E}\left[W_{11}^{(2)}\right]\mathbb{E}\left[W_{11}^{(2)}\phi'(Z_1^{(2)})\right] \\ &\quad + \text{var}\left(\phi'(Z_1^{(3)})\right)\mathbb{E}\left[W_{11}^{(2)}\phi'(Z_1^{(2)})\right]^2 \\ &\quad + \text{var}\left(W_{11}^{(2)}\phi'(Z_1^{(2)})\right)\mathbb{E}\left[\phi'(Z_1^{(3)})\right]^2,\end{aligned}\tag{19}$$

where

$$\begin{aligned}
\text{var} \left(W_{11}^{(2)} \phi'(Z_1^{(2)}) \right) &= \text{var} \left(W_{11}^{(2)} \right) \text{var} \left(\phi'(Z_1^{(2)}) \right) + \underbrace{\text{cov} \left(W_{11}^{(2)}, \phi'(Z_1^{(2)}) \right)^2}_{\text{Eq. 9}} \\
&+ 2 \text{cov} \left(W_{11}^{(2)}, \phi'(Z_1^{(2)}) \right) \mathbb{E} \left[W_{11}^{(2)} \right] \mathbb{E} \left[\phi'(Z_1^{(2)}) \right] \\
&+ \text{var} \left(W_{11}^{(2)} \right) \mathbb{E} \left[\phi'(Z_1^{(2)}) \right]^2 + \text{var} \left(\phi'(Z_1^{(2)}) \right) \mathbb{E} \left[W_{11}^{(2)} \right]^2 \\
&= \text{var} \left(W_{11}^{(2)} \right) \text{var} \left(\phi'(Z_1^{(2)}) \right) + \text{var} \left(W_{11}^{(2)} \right) \mathbb{E} \left[\phi'(Z_1^{(2)}) \right]^2 \\
&+ \text{var} \left(\phi'(Z_1^{(2)}) \right) \mathbb{E} \left[W_{11}^{(2)} \right]^2.
\end{aligned} \tag{20}$$

B.3.2 Partial Derivative $\frac{\partial A_1^{(3)}}{\partial Z_1^{(1)}}$

This section presents the calculations of the partial derivative of $A_1^{(3)}$ with respect to $Z_1^{(1)}$. According to the partial derivative diagram, there are two branches relating to this partial derivative. The partial derivative is a sum of the product of partial derivatives on these two branches. The rest of this section only presents the computations for one of these two branches (Figure 11). This partial derivative is defined following

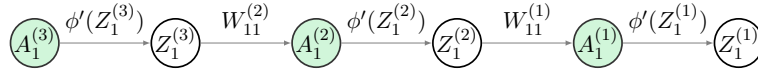


Figure 11: Illustration of a branch of partial derivative of $A_1^{(3)}$ with respect to $Z_1^{(1)}$.

$$\frac{\partial A_1^{(3)}}{\partial Z_1^{(1)}} = \phi'(Z_1^{(3)}) W_{11}^{(2)} \phi'(Z_1^{(2)}) W_{11}^{(1)} \phi'(Z_1^{(1)}). \tag{21}$$

The expected value is computed using Equation 11, 12, 9 and 16,

$$\begin{aligned}
\mathbb{E} \left[\frac{\partial A_1^{(3)}}{\partial Z_1^{(1)}} \right] &= \mathbb{E} \left[\phi'(Z_1^{(3)}) W_{11}^{(2)} \phi'(Z_1^{(2)}) W_{11}^{(1)} \phi'(Z_1^{(1)}) \right] \\
&= \mathbb{E} \left[\phi'(Z_1^{(3)}) W_{11}^{(2)} \phi'(Z_1^{(2)}) \right] \mathbb{E} \left[W_{11}^{(1)} \phi'(Z_1^{(1)}) \right] \\
&\quad + \text{cov} \left(\phi'(Z_1^{(3)}) W_{11}^{(2)} \phi'(Z_1^{(2)}), W_{11}^{(1)} \phi'(Z_1^{(1)}) \right),
\end{aligned} \tag{22}$$

where

$$\mathbb{E} \left[W_{11}^{(1)} \phi'(Z_1^{(1)}) \right] = \mathbb{E} \left[W_{11}^{(1)} \right] \mathbb{E} \left[\phi'(Z_1^{(1)}) \right] + \text{cov} \left(W_{11}^{(1)}, \phi'(Z_1^{(1)}) \right), \tag{23}$$

$$\begin{aligned}
&\text{cov} \left(\phi'(Z_1^{(3)}) W_{11}^{(2)} \phi'(Z_1^{(2)}), W_{11}^{(1)} \phi'(Z_1^{(1)}) \right) \\
&= \text{cov} \left(\phi'(Z_1^{(3)}), W_{11}^{(1)} \phi'(Z_1^{(1)}) \right) \mathbb{E} \left[W_{11}^{(2)} \phi'(Z_1^{(2)}) \right] \\
&\quad + \text{cov} \left(W_{11}^{(2)} \phi'(Z_1^{(2)}), W_{11}^{(1)} \phi'(Z_1^{(1)}) \right) \mathbb{E} \left[\phi'(Z_1^{(3)}) \right] \\
&= \left\{ \text{cov} \left(\phi'(Z_1^{(2)}), W_{11}^{(1)} \phi'(Z_1^{(1)}) \right) \mathbb{E} \left[W_{11}^{(2)} \right] \right. \\
&\quad \left. + \text{cov} \left(W_{11}^{(2)}, W_{11}^{(1)} \phi'(Z_1^{(1)}) \right) \mathbb{E} \left[\phi'(Z_1^{(2)}) \right] \right\} \mathbb{E} \left[\phi'(Z_1^{(3)}) \right] \\
&= \text{cov} \left(\phi'(Z_1^{(2)}), W_{11}^{(1)} \phi'(Z_1^{(1)}) \right) \mathbb{E} \left[W_{11}^{(2)} \right] \mathbb{E} \left[\phi'(Z_1^{(3)}) \right], \\
&\text{cov} \left(\phi'(Z_1^{(2)}), W_{11}^{(1)} \phi'(Z_1^{(1)}) \right) \\
&= \text{cov} \left(\phi'(Z_1^{(2)}), W_{11}^{(1)} \right) \mathbb{E} \left[\phi'(Z_1^{(1)}) \right] \\
&\quad + \text{cov} \left(\phi'(Z_1^{(2)}), \phi'(Z_1^{(1)}) \right) \mathbb{E} \left[W_{11}^{(1)} \right].
\end{aligned} \tag{24}$$

The variance is computed using Equation 14, 16, 19, 23, and 24,

$$\begin{aligned}
\text{var} \left(\frac{\partial A_1^{(3)}}{\partial Z_1^{(1)}} \right) &= \text{var} \left(\phi'(Z_1^{(3)}) W_{11}^{(2)} \phi'(Z_1^{(2)}) W_{11}^{(1)} \phi'(Z_1^{(1)}) \right) \\
&= \text{var} \left(\phi'(Z_1^{(3)}) W_{11}^{(2)} \phi'(Z_1^{(2)}) \right) \text{var} \left(W_{11}^{(1)} \phi'(Z_1^{(1)}) \right) \\
&+ \text{cov} \left(\phi'(Z_1^{(3)}) W_{11}^{(2)} \phi'(Z_1^{(2)}), W_{11}^{(1)} \phi'(Z_1^{(1)}) \right)^2 \\
&+ 2\text{cov} \left(\phi'(Z_1^{(3)}) W_{11}^{(2)} \phi'(Z_1^{(2)}), W_{11}^{(1)} \phi'(Z_1^{(1)}) \right) \quad (25) \\
&\quad \mathbb{E} \left[\phi'(Z_1^{(3)}) W_{11}^{(2)} \phi'(Z_1^{(2)}) \right] \mathbb{E} \left[W_{11}^{(1)} \phi'(Z_1^{(1)}) \right] \\
&+ \text{var} \left(\phi'(Z_1^{(3)}) W_{11}^{(2)} \phi'(Z_1^{(2)}) \right) \mathbb{E} \left[W_{11}^{(1)} \phi'(Z_1^{(1)}) \right]^2 \\
&+ \text{var} \left(W_{11}^{(1)} \phi'(Z_1^{(1)}) \right) \mathbb{E} \left[\phi'(Z_1^{(3)}) W_{11}^{(2)} \phi'(Z_1^{(2)}) \right]^2.
\end{aligned}$$

The same above steps are repeated for the second branch in order to complete the calculation of the partial derivative of $A_1^{(3)}$ with respect to $Z_1^{(1)}$.

B.3.3 Partial Derivative $\frac{\partial A_1^{(3)}}{\partial Z_1^{(0)}}$

This section presents the calculations of the partial derivative of $A_1^{(3)}$ with respect to $Z_1^{(0)}$. From the partial derivative diagram (Figure 8), we identify six branches relating to this partial derivative. Therefore, the partial derivative is equal to the sum of the product of partial derivatives on these six branches. Figure 12 shows the details for one of six branches. The partial derivative

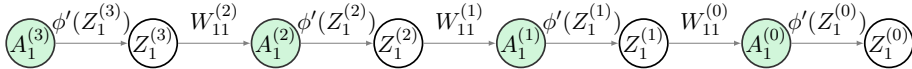


Figure 12: Illustration of a branch of the partial derivative of $A_1^{(3)}$ with respect to $Z_1^{(0)}$.

relating to this branch is defined following

$$\frac{\partial A_1^{(3)}}{\partial Z_1^{(0)}} = \phi'(Z_1^{(3)}) W_{11}^{(2)} \phi'(Z_1^{(2)}) W_{11}^{(1)} \phi'(Z_1^{(1)}) W_{11}^{(0)} \phi'(Z_1^{(0)}). \quad (26)$$

The expected value is computed using Equation 11, 9 and 22,

$$\begin{aligned}
\mathbb{E} \left[\frac{\partial A_1^{(3)}}{\partial Z_1^{(0)}} \right] &= \mathbb{E} \left[\phi'(Z_1^{(3)}) W_{11}^{(2)} \phi'(Z_1^{(2)}) W_{11}^{(1)} \phi'(Z_1^{(1)}) W_{11}^{(0)} \phi'(Z_1^{(0)}) \right] \\
&= \mathbb{E} \left[\phi'(Z_1^{(3)}) W_{11}^{(2)} \phi'(Z_1^{(2)}) W_{11}^{(1)} \phi'(Z_1^{(1)}) \right] \mathbb{E} \left[W_{11}^{(0)} \phi'(Z_1^{(0)}) \right] \\
&\quad + \text{cov} \left(\phi'(Z_1^{(3)}) W_{11}^{(2)} \phi'(Z_1^{(2)}) W_{11}^{(1)} \phi'(Z_1^{(1)}), W_{11}^{(0)} \phi'(Z_1^{(0)}) \right), \tag{27}
\end{aligned}$$

where

$$\mathbb{E} \left[W_{11}^{(0)} \phi'(Z_1^{(0)}) \right] = \mathbb{E} \left[W_{11}^{(0)} \right] \mathbb{E} \left[\phi'(Z_1^{(0)}) \right] + \text{cov} \left(W_{11}^{(1)}, \phi'(Z_1^{(0)}) \right), \tag{28}$$

$$\begin{aligned}
&\text{cov} \left(\phi'(Z_1^{(3)}) W_{11}^{(2)} \phi'(Z_1^{(2)}) W_{11}^{(1)} \phi'(Z_1^{(1)}), W_{11}^{(0)} \phi'(Z_1^{(0)}) \right) \\
&= \text{cov} \left(\phi'(Z_1^{(3)}) W_{11}^{(2)} \phi'(Z_1^{(2)}), W_{11}^{(0)} \phi'(Z_1^{(0)}) \right) \\
&\quad \times \mathbb{E} \left[W_{11}^{(0)} \phi'(Z_1^{(0)}) \right] \\
&\quad + \text{cov} \left(W_{11}^{(1)} \phi'(Z_1^{(1)}), W_{11}^{(0)} \phi'(Z_1^{(0)}) \right) \\
&\quad \times \mathbb{E} \left[\phi'(Z_1^{(3)}) W_{11}^{(2)} \phi'(Z_1^{(2)}) \right] \\
&= \text{cov} \left(\phi'(Z_1^{(1)}), W_{11}^{(0)} \phi'(Z_1^{(0)}) \right) \\
&\quad \times \mathbb{E} \left[W_{11}^{(1)} \right] \underbrace{\mathbb{E} \left[\phi'(Z_1^{(3)}) W_{11}^{(2)} \phi'(Z_1^{(2)}) \right]}_{\text{Eq. (16)}} \\
&\text{cov} \left(\phi'(Z_1^{(1)}), W_{11}^{(0)} \phi'(Z_1^{(0)}) \right) \\
&= \text{cov} \left(\phi'(Z_1^{(1)}), W_{11}^{(0)} \right) \mathbb{E} \left[\phi'(Z_1^{(0)}) \right] \\
&\quad + \text{cov} \left(\phi'(Z_1^{(1)}), \phi'(Z_1^{(0)}) \right) \mathbb{E} \left[W_{11}^{(0)} \right]. \tag{29}
\end{aligned}$$

The variance is computed using Equation 14, 22, 25, 28 and 29,

$$\begin{aligned}
\text{var} \left(\frac{\partial A_1^{(3)}}{\partial Z_1^{(0)}} \right) &= \text{var} \left(\phi'(Z_1^{(3)})W_{11}^{(2)}\phi'(Z_1^{(2)})W_{11}^{(1)}\phi'(Z_1^{(1)})W_{11}^{(0)}\phi'(Z_1^{(0)}) \right) \\
&= \text{var} \left(\phi'(Z_1^{(3)})W_{11}^{(2)}\phi'(Z_1^{(2)})W_{11}^{(1)}\phi'(Z_1^{(1)}) \right) \text{var} \left(W_{11}^{(0)}\phi'(Z_1^{(0)}) \right) \\
&\quad + \text{cov} \left(\phi'(Z_1^{(3)})W_{11}^{(2)}\phi'(Z_1^{(2)})W_{11}^{(1)}\phi'(Z_1^{(1)}), W_{11}^{(0)}\phi'(Z_1^{(0)}) \right)^2 \\
&\quad + 2\text{cov} \left(\phi'(Z_1^{(3)})W_{11}^{(2)}\phi'(Z_1^{(2)})W_{11}^{(1)}\phi'(Z_1^{(1)}), W_{11}^{(0)}\phi'(Z_1^{(0)}) \right) \\
&\quad \times \mathbb{E} \left[\phi'(Z_1^{(3)})W_{11}^{(2)}\phi'(Z_1^{(2)})W_{11}^{(1)}\phi'(Z_1^{(1)}) \right] \mathbb{E} \left[W_{11}^{(0)}\phi'(Z_1^{(0)}) \right] \\
&\quad + \text{var} \left(\phi'(Z_1^{(3)})W_{11}^{(2)}\phi'(Z_1^{(2)})W_{11}^{(1)}\phi'(Z_1^{(1)}) \right) \mathbb{E} \left[W_{11}^{(0)}\phi'(Z_1^{(0)}) \right]^2 \\
&\quad + \text{var} \left(W_{11}^{(0)}\phi'(Z_1^{(0)}) \right) \mathbb{E} \left[\phi'(Z_1^{(3)})W_{11}^{(2)}\phi'(Z_1^{(2)})W_{11}^{(1)}\phi'(Z_1^{(1)}) \right]^2.
\end{aligned} \tag{30}$$

The same calculations are repeated for the five remaining branches in order to obtain the partial derivative of $A_1^{(3)}$ with respect to $Z_1^{(0)}$.

B.3.4 Covariance between $\frac{\partial A_1^{(3)}}{\partial Z_1^{(0)}}$ and $Z_1^{(0)}$

This section presents the calculations of the covariance for the partial derivative $\frac{\partial A_1^{(3)}}{\partial Z_1^{(0)}}$ and $Z_1^{(0)}$. The following calculations correspond to the branch illustrated in Figure 12,

$$\begin{aligned}
&\text{cov} \left(\frac{\partial A_1^{(3)}}{\partial Z_1^{(0)}}, Z_1^{(0)} \right) \\
&= \text{cov} \left(\phi'(Z_1^{(3)})W_{11}^{(2)}\phi'(Z_1^{(2)})W_{11}^{(1)}\phi'(Z_1^{(1)})W_{11}^{(0)}\phi'(Z_1^{(0)}), Z_1^{(0)} \right) \\
&= \text{cov} \left(\phi'(Z_1^{(3)})W_{11}^{(2)}\phi'(Z_1^{(2)})W_{11}^{(1)}\phi'(Z_1^{(1)}), Z_1^{(0)} \right) \underbrace{\mathbb{E} \left[W_{11}^{(0)}\phi'(Z_1^{(0)}) \right]}_{\text{Eq. (28)}} \\
&\quad + \text{cov} \left(W_{11}^{(0)}\phi'(Z_1^{(0)}), Z_1^{(0)} \right) \underbrace{\mathbb{E} \left[\phi'(Z_1^{(3)})W_{11}^{(2)}\phi'(Z_1^{(2)})W_{11}^{(1)}\phi'(Z_1^{(1)}) \right]}_{\text{Eq. (22)}},
\end{aligned} \tag{31}$$

where

$$\begin{aligned}
& \text{cov} \left(\phi'(Z_1^{(3)})W_{11}^{(2)}\phi'(Z_1^{(2)})W_{11}^{(1)}\phi'(Z_1^{(1)}), Z_1^{(0)} \right) \\
&= \text{cov} \left(\phi'(Z_1^{(3)})W_{11}^{(2)}\phi'(Z_1^{(2)}), Z_1^{(0)} \right) \mathbb{E} \left[W_{11}^{(1)}\phi'(Z_1^{(1)}) \right] \\
&+ \text{cov} \left(W_{11}^{(1)}\phi'(Z_1^{(1)}), Z_1^{(0)} \right) \mathbb{E} \left[\phi'(Z_1^{(3)})W_{11}^{(2)}\phi'(Z_1^{(2)}) \right] \\
&= \left\{ \text{cov} \left(W_{11}^{(1)}, Z_1^{(0)} \right) \mathbb{E} \left[\phi'(Z_1^{(1)}) \right] \right. \\
&+ \left. \text{cov} \left(\phi'(Z_1^{(1)}), Z_1^{(0)} \right) \mathbb{E} \left[W_{11}^{(1)} \right] \right\} \mathbb{E} \left[\phi'(Z_1^{(3)})W_{11}^{(2)}\phi'(Z_1^{(2)}) \right] \\
&= \text{cov} \left(\phi'(Z_1^{(1)}), Z_1^{(0)} \right) \mathbb{E} \left[W_{11}^{(1)} \right] \underbrace{\mathbb{E} \left[\phi'(Z_1^{(3)})W_{11}^{(2)}\phi'(Z_1^{(2)}) \right]}_{\text{Eq. (16)}}
\end{aligned} \tag{32}$$

$$\begin{aligned}
\text{cov} \left(W_{11}^{(0)}\phi'(Z_1^{(0)}), Z_1^{(0)} \right) &= \text{cov} \left(W_{11}^{(0)}, Z_1^{(0)} \right) \mathbb{E} \left[\phi'(Z_1^{(0)}) \right] \\
&+ \text{cov} \left(\phi'(Z_1^{(0)}), Z_1^{(0)} \right) \mathbb{E} \left[W_{11}^{(0)} \right].
\end{aligned} \tag{33}$$

Note that the formulations for $\text{cov} \left(\phi'(Z_1^{(1)}), Z_1^{(0)} \right)$ and $\text{cov} \left(\phi'(Z_1^{(0)}), Z_1^{(0)} \right)$ are provided in §B.5. As mentioned in §B.3.3, there are six branches relating to $\frac{\partial A_1^{(3)}}{\partial Z_1^{(0)}}$. Therefore, we apply the same calculations for the five remaining branches. The final covariance between $\frac{\partial A_1^{(3)}}{\partial Z_1^{(0)}}$ and $Z_1^{(0)}$ is equal to the sum of the covariance of these branches.

B.4 Generalization

This section presents the generalized formulations for a branch of the partial derivative diagram for a feedforward neural networks relating to the partial derivative of an activation unit at layer L, i.e., $A^{(L)}$ with respect to a hidden state at layer l , i.e., $Z^{(l)}$. Figure 13 shows a branch of the partial derivative diagram for a FNN.

B.4.1 Partial Derivative

$$\frac{\partial a^{(L)}}{\partial z^{(l)}} = X^{(L)}Y^{(L-1)}X^{(L-1)} \dots Y^{(l+1)}X^{(l+1)}Y^{(l)}X^{(l)} \tag{34}$$

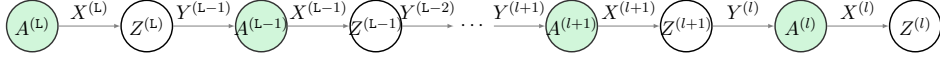


Figure 13: Illustration of a branch in the partial derivative diagram.

The expected value is computed following

$$\begin{aligned} \mathbb{E} \left[\frac{\partial a^{(L)}}{\partial z^{(l)}} \right] &= \underbrace{\mathbb{E} \left[X^{(L)} Y^{(L-1)} X^{(L-1)} \dots Y^{(l+1)} X^{(l+1)} \right]}_{\mathbb{E} \left[\frac{\partial a^{(L)}}{\partial z^{(l+1)}} \right]} \mathbb{E} [Y^{(l)}] \mathbb{E} [X^{(l)}] \\ &+ \text{cov} \left(X^{(L)} Y^{(L-1)} X^{(L-1)} \dots Y^{(l+1)} X^{(l+1)}, Y^{(l)} X^{(l)} \right), \end{aligned} \quad (35)$$

where

$$\begin{aligned} &\text{cov} \left(X^{(L)} Y^{(L-1)} X^{(L-1)} \dots Y^{(l+1)} X^{(l+1)}, Y^{(l)} X^{(l)} \right) \\ &= \{ \text{cov} \left(X^{(l+1)}, Y^{(l)} \right) \mathbb{E} [X^{(l)}] \\ &+ \text{cov} \left(X^{(l+1)}, X^{(l)} \right) \mathbb{E} [Y^{(l)}] \} \\ &\times \underbrace{\mathbb{E} [Y^{(l+1)}] \mathbb{E} \left[X^{(L)} Y^{(L-1)} X^{(L-1)} \right]}_{\mathbb{E} \left[\frac{\partial a^{(L)}}{\partial z^{(L-1)}} \right]}. \end{aligned} \quad (36)$$

The variance is computed following

$$\begin{aligned} \text{var} \left(\frac{\partial a^{(L)}}{\partial z^{(l)}} \right) &= \underbrace{\text{var} \left(X^{(L)} Y^{(L-1)} X^{(L-1)} \dots Y^{(l+1)} X^{(l+1)} \right)}_{\text{var} \left(\frac{\partial a^{(L)}}{\partial z^{(l+1)}} \right)} \text{var} \left(Y^{(l)} X^{(l)} \right) \\ &+ \text{cov} \left(X^{(L)} Y^{(L-1)} X^{(L-1)} \dots Y^{(l+1)} X^{(l+1)}, Y^{(l)} X^{(l)} \right)^2 \\ &+ 2 \text{cov} \left(X^{(L)} Y^{(L-1)} X^{(L-1)} \dots Y^{(l+1)} X^{(l+1)}, Y^{(l)} X^{(l)} \right) \\ &\times \underbrace{\mathbb{E} \left[X^{(L)} Y^{(L-1)} X^{(L-1)} \dots Y^{(l+1)} X^{(l+1)} \right]}_{\mathbb{E} \left[\frac{\partial a^{(L)}}{\partial z^{(l+1)}} \right]} \mathbb{E} [Y^{(l)}] \mathbb{E} [X^{(l)}] \\ &+ \text{var} \left(X^{(L)} Y^{(L-1)} X^{(L-1)} \dots Y^{(l+1)} X^{(l+1)} \right) \mathbb{E} [Y^{(l)}]^2 \mathbb{E} [X^{(l)}]^2 \\ &+ \text{var} \left(Y^{(l)} X^{(l)} \right) \mathbb{E} \left[X^{(L)} Y^{(L-1)} X^{(L-1)} \dots Y^{(l+1)} X^{(l+1)} \right]^2. \end{aligned} \quad (37)$$

B.4.2 Covariance between Partial Derivative and Hidden State

$$\begin{aligned}
& \text{cov} \left(\frac{\partial a^{(L)}}{\partial z^{(l)}}, z^{(l)} \right) \\
&= \text{cov} \left(X^{(l+1)}, z^{(l)} \right) \mathbb{E} [Y^{(l+1)}] \mathbb{E} [Y^{(l)}] \mathbb{E} [X^{(l)}] \underbrace{\mathbb{E} \left[X^{(L)} Y^{(L-1)} X^{(L-1)} \right]}_{\mathbb{E} \left[\frac{\partial a^{(L)}}{\partial z^{(L-1)}} \right]} \\
&+ \text{cov} \left(X^{(l)}, z^{(l)} \right) \mathbb{E} [Y^{(l)}] \underbrace{\mathbb{E} \left[X^{(L)} Y^{(L-1)} X^{(L-1)} \dots Y^{(l+1)} X^{(l+1)} \right]}_{\mathbb{E} \left[\frac{\partial a^{(L)}}{\partial z^{(l+1)}} \right]}.
\end{aligned} \tag{38}$$

B.5 Activation Function

B.5.1 Tanh(Z)

The derivative of the function $\phi(Z) = \tanh(Z)$ with respect to the hidden state Z is written as

$$\phi'(Z) = \frac{d\phi(z)}{dz} = 1 - \phi(Z)^2. \tag{39}$$

The expected value of $\phi'(Z_j^{(l)})$ is computed using Equation 11 and 39

$$\begin{aligned}
\mathbb{E} [\phi'(z)] &= \mathbb{E} \left[1 - \phi(Z_j^{(l)})^2 \right] \\
&= 1 - \mathbb{E} \left[\phi \left(Z_j^{(l)} \right) \right]^2 - \text{var} \left(\phi(Z_j^{(l)}) \right).
\end{aligned} \tag{40}$$

The variance of $\phi'(Z_j^{(l)})$ is computed using Equation 14

$$\begin{aligned}
\text{var} \left(\phi'(Z_j^{(l)}) \right) &= \text{var} \left(1 - \phi(Z_j^{(l)})^2 \right) \\
&= \text{var} \left(\phi(Z_j^{(l)})^2 \right) \\
&= 2 \text{var} \left(\phi(Z_j^{(l)}) \right) \left\{ \text{var} \left(Z_j^{(l)} \right) + 2 \mathbb{E} \left[\phi(Z_j^{(l)}) \right]^2 \right\}.
\end{aligned} \tag{41}$$

The covariance between $\phi(Z_i^{(l+1)})$ and $W_{ij}^{(l)}$ is computed using Equation 12

$$\begin{aligned}
\text{cov}\left(\phi'(Z_i^{(l+1)}), W_{ij}^{(l)}\right) &= \text{cov}\left(1 - \phi(Z_i^{(l+1)})^2, W_{ij}^{(l)}\right) \\
&= -\text{cov}\left(\phi(Z_i^{(l+1)})^2, W_{ij}^{(l)}\right) \\
&= -2 \text{cov}\left(\phi(Z_i^{(l+1)}), W_{ij}^{(l)}\right) \mathbb{E}\left[\phi(Z_i^{(l+1)})\right].
\end{aligned} \tag{42}$$

Using Equation 8 and 10, Equation 42 is rewritten as

$$\begin{aligned}
\text{cov}\left(\phi'(Z_i^{(l+1)}), W_{ij}^{(l)}\right) &= -2 \text{cov}\left(J_i^{(l+1)}(Z_i^{(l+1)} - \mu_{Z_i}^{(l+1)}) + \phi(\mu_{Z_i}^{(l+1)}), W_{ij}^{(l)}\right) \mathbb{E}\left[\phi(Z_i^{(l+1)})\right] \\
&= -2 J_i^{(l+1)} \text{cov}\left(Z_i^{(l+1)}, W_{ij}^{(l)}\right) \mathbb{E}\left[\phi(Z_i^{(l+1)})\right] \\
&= -2 J_i^{(l+1)} \text{cov}\left(\sum_k W_{ik}^{(l)} \phi(Z_k^{(l)}) + B_i^{(l)}, W_{ij}^{(l)}\right) \mathbb{E}\left[\phi(Z_i^{(l+1)})\right] \\
&= -2 J_i^{(l+1)} \text{cov}\left(W_{ij}^{(l)}, W_{ij}^{(l)}\right) \mathbb{E}\left[\phi(Z_i^{(l)})\right] \mathbb{E}\left[\phi(Z_i^{(l+1)})\right].
\end{aligned} \tag{43}$$

The covariance between $\phi'(Z_j^{(l+1)})$ and $\phi'(Z_i^{(l)})$ is obtained using Equation 13, 8, 9, and 10,

$$\begin{aligned}
\text{cov}\left(\phi'(Z_i^{(l+1)}), \phi'(Z_j^{(l)})\right) &= \text{cov}\left(1 - \phi(Z_i^{(l+1)})^2, 1 - \phi(Z_j^{(l)})^2\right) \\
&= \text{cov}\left(\phi(Z_i^{(l+1)})^2, \phi(Z_j^{(l)})^2\right) \\
&= 2 \text{cov}\left(\phi(Z_i^{(l+1)}), \phi(Z_j^{(l)})\right)^2 \\
&+ 4 \text{cov}\left(\phi(Z_i^{(l+1)}), \phi(Z_j^{(l)})\right) \mathbb{E}\left[\phi(Z_i^{(l+1)})\right] \mathbb{E}\left[\phi(Z_j^{(l)})\right],
\end{aligned} \tag{44}$$

where

$$\begin{aligned}
\text{cov} \left(\phi(Z_i^{(l+1)}), \phi(Z_j^{(l)}) \right) &= J_i^{(l+1)} \text{cov} \left(\sum_k W_{ik}^{(l)} \phi(Z_k^{(l)}) + B_i^{(l)}, \phi(Z_i^{(l)}) \right) \\
&= J_i^{(l+1)} \text{cov} \left(W_{ij}^{(l)} \phi(Z_j^{(l)}), \phi(Z_i^{(l)}) \right) \\
&= J_i^{(l+1)} \text{cov} \left(\phi(Z_j^{(l)}), \phi(Z_i^{(l)}) \right) \mathbb{E} \left[W_{ij}^{(l)} \right] \\
&+ \cancel{J_i^{(l+1)} \text{cov} \left(W_{ij}^{(l)}, \phi(Z_i^{(l)}) \right) \mathbb{E} \left[\phi(Z_j^{(l)}) \right]}^0.
\end{aligned} \tag{45}$$

The covariance between $\phi'(Z_i^{(l+1)})$ and $Z_j^{(l)}$ is computed using Equation 12, 8, 9, and 10,

$$\begin{aligned}
\text{cov} \left(\phi'(Z_i^{(l+1)}), Z_j^{(l)} \right) &= \text{cov} \left(1 - \phi(Z_i^{(l+1)})^2, Z_j^{(l)} \right) \\
&= -2 \text{cov} \left(\phi(Z_i^{(l+1)}), Z_j^{(l)} \right) \mathbb{E} \left[Z_j^{(l)} \right] \\
&= -2 J_i^{(l+1)} \text{cov} \left(\sum_k W_{ik}^{(l)} \phi(Z_k^{(l)}) + B_i^{(l)}, Z_j^{(l)} \right) \mathbb{E} \left[Z_j^{(l)} \right] \\
&= -2 J_i^{(l+1)} \text{cov} \left(W_{ij}^{(l)} \phi(Z_j^{(l)}), Z_j^{(l)} \right) \mathbb{E} \left[Z_j^{(l)} \right] \\
&= -2 J_i^{(l+1)} \text{cov} \left(\phi(Z_j^{(l)}), Z_j^{(l)} \right) \mathbb{E} \left[W_{ij}^{(l)} \right] \mathbb{E} \left[Z_j^{(l)} \right] \\
&- \cancel{2 J_i^{(l+1)} \text{cov} \left(W_{ij}^{(l)}, Z_j^{(l)} \right) \mathbb{E} \left[\phi(Z_j^{(l)}) \right] \mathbb{E} \left[Z_j^{(l)} \right]}^0 \\
&= 2 J_i^{(l+1)} J_j^{(l)} \text{cov} \left(Z_j^{(l)}, Z_j^{(l)} \right) \mathbb{E} \left[W_{ij}^{(l)} \right] \mathbb{E} \left[Z_j^{(l)} \right].
\end{aligned} \tag{46}$$

The covariance between $\phi'(Z_j^{(l)})$ and $Z_j^{(l)}$ is computed using Equation 12

$$\begin{aligned}
\text{cov} \left(\phi'(Z_j^{(l)}), Z_j^{(l)} \right) &= \text{cov} \left(1 - \phi(Z_j^{(l)})^2, Z_j^{(l)} \right) \\
&= -2 \text{cov} \left(\phi(Z_j^{(l)}), Z_j^{(l)} \right) \mathbb{E} \left[\phi(Z_j^{(l)}) \right] \\
&= -2 J_j^{(l)} \text{cov} \left(Z_j^{(l)}, Z_j^{(l)} \right) \mathbb{E} \left[\phi(Z_j^{(l)}) \right].
\end{aligned} \tag{47}$$

B.5.2 ReLU(\mathbf{Z})

The derivative of the function $\phi(Z) = \text{ReLU}(Z)$ with respect to the hidden state Z and its covariance are formulated following

$$\begin{aligned}\phi'(Z) &= \begin{cases} 1 & \text{if } \mathbb{E}[Z] > 0 \\ 0 & \text{if } \mathbb{E}[Z] \leq 0. \end{cases} \\ \mathbb{E}[\phi'(Z_j^{(l)})] &= 1 \\ \text{var}(\phi'(Z_j^{(l)})) &= 0 \\ \text{cov}(\phi'(Z_i^{(l+1)}), W_{ij}^{(l)}) &= 0 \\ \text{cov}(\phi'(Z_i^{(l+1)}), \phi'(Z_j^{(l)})) &= 0 \\ \text{cov}(\phi'(Z_i^{(l+1)}), Z_j^{(l)}) &= 0 \\ \text{cov}(\phi'(Z_j^{(l)}), Z_j^{(l)}) &= 0. \end{aligned} \tag{48}$$